

FAR-ULTRAVIOLET SPECTROSCOPIC EXPLORER OBSERVATIONS OF DEGREE-SCALE VARIATIONS IN GALACTIC HALO O VI

J. CHRISTOPHER HOWK,¹ BLAIR D. SAVAGE,² KENNETH R. SEMBACH,^{1,3} AND CHARLES G. HOOPES¹

Received 2001 December 11; accepted 2002 February 12

ABSTRACT

We report *Far-Ultraviolet Spectroscopic Explorer (FUSE)* observations of interstellar O VI absorption in the halo of the Milky Way toward 12 early-type stars in the Large Magellanic Cloud (LMC) and 11 in the Small Magellanic Cloud (SMC). The mean column densities of O VI associated with the Galactic halo toward the LMC and SMC are $\log\langle N(\text{O VI}) \rangle = 14.52^{+0.10}_{-0.14}$ and $14.13^{+0.14}_{-0.20}$, respectively, where the uncertainties represent the standard deviations of the individual measurements about the means. Significant variations in the O VI column densities are observed over all of the angular scales probed by our observations: $0^\circ\text{--}5^\circ$ toward the LMC and $0^\circ\text{--}3^\circ$ toward the SMC. The maximum factors by which the O VI varies between sight lines toward the LMC and SMC are ~ 2.8 and ~ 4.2 , respectively. Although low-, intermediate-, and high-velocity clouds are present along most of the sight lines toward the LMC, the variations in O VI column densities are found in all of these O VI absorbing structures. The column density variations trace the structure of the hot ionized medium in the Galactic halo on scales of $\ll 80\text{--}800$ pc toward the LMC and $\ll 6\text{--}400$ pc toward the SMC (assuming that the absorption arises within the first 5 kpc above the Galactic plane).

Subject headings: ISM: atoms — ISM: structure — ultraviolet: ISM

1. INTRODUCTION

Observations of absorption from O VI in the interstellar medium (ISM) toward early-type stars and extragalactic objects provide a useful means of studying the hot gaseous medium of galaxies. Because 113.9 eV are required to ionize O V to O VI, photoionization is unlikely produce the observed quantities of O VI in galactic environments (see Savage et al. 2000; Sembach et al. 2000). This fact, coupled with the high intrinsic abundance of O and the strength of the O VI absorption doublet at 1031.926 and 1037.617 Å, makes this ion a sensitive probe of the conditions of the hot ISM in the Milky Way and other nearby galaxies.

The *Far-Ultraviolet Spectroscopic Explorer (FUSE)*, launched in 1999 June, is producing a large database of high-resolution ($R \sim 15,000\text{--}20,000$) spectra covering the far-ultraviolet (FUV) wavelength range 905–1187 Å, which includes the important O VI doublet. *FUSE* can easily observe stars in the Galactic halo, stars in the Magellanic Clouds, and distant extragalactic sources with sufficient signal-to-noise ratio to produce reliable O VI column density and line profile measurements. Early reports of *FUSE* observations include studies of interstellar O VI absorption in the Galactic halo (Savage et al. 2000; Oegerle et al. 2000), in high-velocity clouds (Sembach et al. 2000; Murphy et al. 2000), and in the Galaxy and the Large Magellanic Cloud toward the star Sk $-67^\circ 05$ (Friedman et al. 2000).

In this paper we discuss *FUSE* observations of interstellar O VI in the halo of the Milky Way as observed toward 12 early-type stars in the Large Magellanic Cloud [LMC; $(l, b) = (280^\circ 5, -32^\circ 9)$; $d = 50$ kpc] and 11 early-type stars in the Small Magellanic Cloud [SMC; $(l, b) = (302^\circ 8,$

$-44^\circ 3)$; $d = 65$ kpc]. These observations have previously been used to study the O VI content of these galaxies (Howk et al. 2002; Hoopes et al. 2002). Our emphasis in this paper is on the degree of variability in the O VI column densities over the small angular scales ($0^\circ\text{--}5^\circ$) probed by these Magellanic Cloud observations.

The remainder of this paper is laid out as follows. In § 2 we discuss the *FUSE* observations and the properties of the sight lines toward each of the Magellanic Clouds. We present the small-scale O VI measurements in § 3, and we briefly discuss the kinematics of the O VI profiles along these directions in § 4. We discuss the implications of these measurements for the highly ionized Galactic halo in § 5 and summarize our results in § 6.

2. FUSE OBSERVATIONS OF THE MAGELLANIC CLOUD SIGHT LINES

2.1. The LMC Sight Line

The first high-resolution UV absorption-line measurements along sight lines toward extragalactic objects were *International Ultraviolet Explorer (IUE)* observations of early-type stars in the LMC (Savage & de Boer 1979). This high-latitude sight line ($b \sim -33^\circ$) probes the thin interstellar disk of the Milky Way only along the first few hundred parsecs ($z \sim 200$ pc at a distance of $d \sim 400$ pc from the Sun). The first ~ 100 pc in this direction are contained within the boundaries of the local bubble, where there is relatively little material (Sfeir et al. 1999). Most of the LMC sight line probes the “thick disk” or “halo” of the Milky Way, and many of the interstellar clouds along this sight line show abundances reminiscent of other Galactic halo clouds (Welty et al. 1999; Friedman et al. 2000). Gas participating in Galactic rotation (Clemens 1985) within the first ~ 5 kpc of the Sun ($z \lesssim 2.5$ kpc) in this direction will be at low negative velocities ($-5 \text{ km s}^{-1} \lesssim v_{\text{LSR}} \lesssim 0 \text{ km s}^{-1}$). More distant gas will be found at positive velocities, reaching $v_{\text{LSR}} \sim +100 \text{ km s}^{-1}$ at 25 kpc ($z \sim 12.5$ kpc).

¹ Department of Physics and Astronomy, The Johns Hopkins University, Baltimore, MD 21218; howk@pha.jhu.edu, choopes@pha.jhu.edu.

² Astronomy Department, University of Wisconsin–Madison, Madison, WI 53711; savage@astro.wisc.edu.

³ Current address: Space Telescope Science Institute, 3700 San Martin Drive, Baltimore, MD 21218; sembach@stsci.edu.

Several clouds or cloud complexes have been identified along the sight line to the LMC, mostly in tracers of neutral gas. McGee, Newton, & Morton (1983) summarize H I 21 cm observations of the cloud complexes in the general direction of the LMC. They find several components toward the LMC. The main emission complexes are seen at $\langle v_{\text{LSR}} \rangle = -32.8, +0.2, +65.5, \text{ and } +131.7 \text{ km s}^{-1}$, where the velocities are a spatial average over the face of the LMC, with spatially averaged H I column densities of 7.1×10^{18} , 4.3×10^{20} , 4.3×10^{18} , and $6.0 \times 10^{18} \text{ atoms cm}^{-2}$. The component nearest the LSR can be associated with local gas in the Galactic disk. The $\langle v_{\text{LSR}} \rangle \sim -33$ and $+65 \text{ km s}^{-1}$ components are referred to as intermediate-velocity clouds (IVCs), while the $\sim +130 \text{ km s}^{-1}$ cloud is cataloged as a high-velocity cloud (HVC). These components can also be seen in metal absorption lines (e.g., Ferlet, Dennefeld, & Marice 1985; Savage & de Boer 1981), including moderately and highly ionized species (Welty et al. 1999; Wakker et al. 1998), and Danforth et al. (2002) have discussed their distribution in *FUSE* observations of metal absorption lines. Each of these aforementioned “components” is likely made up of several individual clouds that are unresolved in many data sets (Welty et al. 1999), and the IVC and HVC complexes probably reside in the Galactic halo (Welty et al. 1999).

The highly ionized gas along the sight line to the LMC at velocities below those associated with the LMC itself likely traces material in the vertically extended Galactic halo. *IUE* observations of C IV and Si IV along LMC sight lines have been presented by Sembach & Savage (1992), Savage et al. (1989), Savage & de Boer (1981), and others, while Bomans et al. (1996) and Wakker et al. (1998) have presented *Hubble Space Telescope* (*HST*) observations of Galactic C IV along LMC sight lines. We also note that Widmann et al. (1998) have derived O VI column densities for the Galactic halo seen toward the LMC using *Orbiting and Retrievable Far and Extreme Ultraviolet Spectrometer* (*ORFEUS*) data. However, high-quality measurements of the highly ionized Galactic material toward the LMC have been sparse.

In this work we discuss the Galactic O VI absorption as observed with *FUSE* toward 12 early-type stars in the LMC. The observations and analysis of the data used in this work are described in detail by Howk et al. (2002, hereafter Paper I), who make use of the observations to study the hot gas content of the LMC. All of the *FUSE* observations used for this work have a resolution of $\lesssim 20 \text{ km s}^{-1}$ (FWHM). The LMC stars used as background continuum sources in Paper I are all either Wolf-Rayet stars or O stars with spectral types earlier than O7 and were chosen to have well-defined continua in the region of interstellar O VI $\lambda 1031.926$ absorption. The (6–0) *P*(3) and (6–0) *R*(4) transitions of molecular hydrogen can overlap Galactic O VI absorption toward the LMC given the rest wavelengths of these lines and the velocity structure of these sight lines. Models for molecular hydrogen transitions that overlap the Galactic O VI absorption have been divided out in the processing of the spectra. The exposure times for the LMC stars ranged from 3.6 to 33 ks per star, yielding signal-to-noise ratios in the range ~ 12 – 25 per resolution element. The continuum placement, molecular hydrogen correction, and other details are described in Paper I.

Table 1 gives the Milky Way O VI column densities derived by integrating the apparent column density, $N_a(v)$, profiles (see Savage & Sembach 1991) of the 1031.926 Å

transition. The $N_a(v)$ profiles themselves are displayed in Figure 1. Table 1 gives the O VI column densities integrated over two ranges (all velocities are approximately at the local standard of rest; see Paper I): the first over the velocity range $|v| \leq 50 \text{ km s}^{-1}$, and the second over the entire velocity range of the Milky Way (the full range is indicated in the last column of Table 1). As discussed in Paper I the separation between the Milky Way and LMC absorption is not always clear. In these cases we adopt an average separation point of $+175 \text{ km s}^{-1}$. The quoted column density errors for the columns integrated over the entire range include the effects of changing the upper velocity limit by $\pm 20 \text{ km s}^{-1}$, which is sufficient to cover the range of separations observed in cases where there is a clear break between the Milky Way and LMC absorption.

The full range of Milky Way velocities likely includes O VI associated with the IVCs and HVCs present along the LMC sight lines. Examining the strongest transitions of Fe II and O I in the *FUSE* bandpass (at 1144.938 and 1039.230 Å, respectively), we find that 11 of the 12 sight lines studied here exhibit IVC absorption, while at least 10 of the 12 contain HVC absorption.⁴ None of the sight lines is simultaneously free of absorption from IVC and HVC material (i.e., absorption from one or the other is seen along all of the sight lines). The column densities derived by integrating over $|v| \leq 50 \text{ km s}^{-1}$ should exclude much of the IVC and HVC absorption.

2.2. The SMC Sight Line

The higher latitude ($b \sim -44^\circ$) sight line to the SMC is more heavily biased toward low-density Galactic halo gas than that toward the LMC. Toward the SMC, gas within $\sim 10 \text{ kpc}$ ($z \lesssim 7 \text{ kpc}$) that is participating in Galactic rotation (Clemens 1985) would be found at negative velocities, and gas within $\sim 20 \text{ kpc}$ of the Sun ($z \lesssim 14 \text{ kpc}$) should be found at velocities $|v_{\text{LSR}}| \lesssim 40 \text{ km s}^{-1}$.

Similar to the case for the LMC, the sight line toward the SMC contains a number of low-ionization Galactic gas clouds or complexes spread over $\sim 65 \text{ km s}^{-1}$ (Welty et al. 1997; Mallouris et al. 2001). Material associated with the disk and low halo of the Galaxy is seen over the range $-25 \leq v_{\text{LSR}} \lesssim +40 \text{ km s}^{-1}$. High-velocity Galactic material, such as that seen toward the LMC, would be blended with SMC material for velocities $v_{\text{LSR}} \gtrsim +60 \text{ km s}^{-1}$.

Observations of the highly ionized material in the direction of the SMC with *IUE* are discussed by Fitzpatrick & Savage (1983) and Fitzpatrick (1984). More recently, Koenigsberger et al. (2001) and Hoopes et al. (2001) have reported on *HST* and *FUSE* observations of the sight line toward HD 5980 in the SMC. These papers include comments on the highly ionized species C IV, Si IV, and O VI in the Galactic halo.

In this work we make use of *FUSE* observations of Galactic O VI toward 11 early-type stars in the SMC. The observations and analysis of the data are described in Hoopes et al. (2002, hereafter Paper II), who use these observations to study the hot gas content of the SMC. The principal proper-

⁴ Danforth et al. (2002) present the absorption-line profiles of several species toward almost 100 stars in the Magellanic Clouds, including the strong Fe II $\lambda 1144.938$ and O I $\lambda 1039.230$ transitions. We direct the reader to that work for better views of the velocity structure of the ISM along the lines of sight studied in this work.

TABLE 1
INTERSTELLAR O VI IN THE HALO OF THE MILKY WAY TOWARD THE LMC

STAR	α (J2000.0)	δ (J2000.0)	(l, b) (deg)	W_λ^b (mÅ)	$\log N(\text{O VI})^a$		v_-, v_+^c (km s ⁻¹)
					(-50, +50)	(v_-, v_+)	
Sk -67°05 ^d	04 50 18.8	-67 39 38.2	278.89, -36.32	249 ± 10	13.79 ± 0.03	14.40 ± 0.05	-50, +180
Sk -67°20	04 55 31.5	-67 30 00.9	278.53, -35.89	324 ± 16	14.11 ± 0.05	14.56 ± 0.05	-35, +175
Sk -66°51	05 03 10.1	-66 40 53.9	277.32, -35.38	317 ± 21	13.97 ± 0.05	14.57 ± 0.05	-25, +180
Sk -67°69	05 14 20.1	-67 08 03.5	277.57, -34.22	200 ± 15	14.00 ± 0.05	14.32 ± 0.04	-40, +160
Sk -68°80	05 26 30.4	-68 50 26.6	279.34, -32.79	164 ± 9	13.61 ± 0.05	14.22 ± 0.09	-15, +140
Sk -70°91	05 27 33.7	-70 36 48.3	281.40, -32.40	377 ± 11	14.11 ± 0.03	14.67 ± 0.06	-40, +175
Sk -66°100	05 27 45.5	-66 55 14.9	277.06, -32.96	308 ± 32	14.15 ± 0.07	14.54 ± 0.06	-35, +175
Sk -67°144	05 30 12.2	-67 26 08.4	277.63, -32.66	333 ± 29	14.23 ± 0.10	14.61 ± 0.07	-40, +175
Sk -71°45	05 31 15.5	-71 04 08.8	281.87, -32.02	322 ± 7	13.94 ± 0.02	14.55 ± 0.04	-30, +185
Sk -69°191	05 34 19.3	-69 45 10.0	280.29, -31.97	352 ± 38	14.23 ± 0.10	14.64 ± 0.08	-30, +175
Sk -67°211	05 35 13.9	-67 33 27.0	277.70, -32.16	294 ± 8	14.14 ± 0.02	14.50 ± 0.02	-50, +185
Sk -66°172	05 37 05.5	-66 21 35.7	276.27, -32.10	283 ± 21	14.01 ± 0.06	14.50 ± 0.05	-45, +195

NOTE.—Units of right ascension are hours, minutes, and seconds, and units of declination are degrees, arcminutes, and arcseconds.

^a O VI column densities for Milky Way material along the observed sight lines with 1 σ error estimates. Two column densities are given for each sight line: one integrated over the velocity range $v = -50$ to $+50$ km s⁻¹, the other integrated over a range v_- to v_+ , where the values of the limits are given in the last column of this table. The errors in the latter case include the effects of varying the upper velocity limit by ± 20 km s⁻¹ (see text). In all cases the column densities have been derived using observations of the 1031.926 Å transition assuming that no unresolved saturation is present. We assume an f -value of $f = 0.1325$ from the theoretical calculations of Yan, Tambasco, & Drake 1998.

^b Equivalent widths for the Milky Way material along the observed sight lines with 1 σ error estimates.

^c Velocity range over which the full Milky Way profile was integrated.

^d The O VI column densities toward Sk -67°05 are taken from Table 2 of Friedman et al. 2000 assuming their “upper” continuum placement. The “lower” continuum placement implies a column density 0.08 dex lower than that quoted.

ties of the data are the same as those described above for the LMC observations.

Table 2 gives the Milky Way O VI column densities derived from an integration of the apparent column density profiles of the 1032.926 Å transition. The O VI $N_a(v)$ profiles for the SMC sight lines are shown in Figure 2. For the SMC sight lines, contamination of the O VI absorption profiles by

H₂ is not as significant as for the LMC sight lines (see Paper II). The H₂ has not been removed before integrating the $N_a(v)$ profiles. The separation between Galactic and SMC O VI absorption is much cleaner along the SMC sight lines than the LMC sight lines. For this reason, the error budget includes the effects of changing the upper integration limit (last column of Table 2) by only ± 5 km s⁻¹.

TABLE 2
INTERSTELLAR O VI IN THE HALO OF THE MILKY WAY TOWARD THE SMC

STAR	α (J2000.0)	δ (J2000.0)	(l, b) (deg)	W_λ^a (mÅ)	$\log N(\text{O VI})^b$		v_-, v_+^c km s ⁻¹
					(-50, +50)	(v_-, v_+)	
AV 15.....	00 46 42.1	-73 24 54.7	303.40, -43.71	109 ± 11	14.04 ± 0.05	-45, +65	
AV 75.....	00 50 32.5	-72 52 36.2	303.03, -44.25	133 ± 14	14.15 ± 0.06	-40, +50	
AV 83.....	00 50 52.0	-72 42 14.5	302.99, -44.42	84 ± 10	13.93 ± 0.06	-50, +40	
AV 95.....	00 51 21.5	-72 44 12.8	302.94, -44.39	129 ± 18	14.14 ± 0.07	-45, +60	
AV 229.....	00 59 27.7	-72 09 55.0	302.07, -44.95	164 ± 4	14.25 ± 0.02	-45, +70	
AV 232.....	00 49 30.0	-72 11 00.0	303.14, -44.94	155 ± 5	14.23 ± 0.02	-60, +65	
AV 235.....	00 59 42.0	-72 45 00.0	302.08, -44.36	100 ± 10	13.98 ± 0.05	-40, +75	
AV 321.....	01 02 57.0	-72 08 09.3	301.69, -44.96	130 ± 7	14.11 ± 0.04	-40, +75	
AV 378.....	01 05 09.4	-72 05 35.0	301.44, -45.00	123 ± 10	14.09 ± 0.04	-40, +70	
AV 423.....	01 07 40.4	-72 50 59.5	301.26, -44.23	61 ± 10	13.77 ± 0.08	-25, +40	
Sk 188.....	01 31 06.0	-73 26 00.0	299.06, -43.40	215 ± 8	14.39 ± 0.02	-65, +85	

NOTE.—Units of right ascension are hours, minutes, and seconds, and units of declination are degrees, arcminutes, and arcseconds.

^a Equivalent widths for the Milky Way material along the observed sight lines with 1 σ error estimates.

^b O VI column densities for Milky Way material along the observed sight lines with 1 σ error estimates. The column densities have been derived using observations of the 1031.926 Å transition assuming no unresolved saturation is present and integrating over the range v_- to v_+ , where the values of the limits are given in the last column of this table. The errors include the effects of varying the upper velocity limit by ± 5 km s⁻¹ (see text). We assume an f -value of $f = 0.1325$ from the theoretical calculations of Yan et al. 1998.

^c Velocity range over which the full Milky Way profile was integrated.

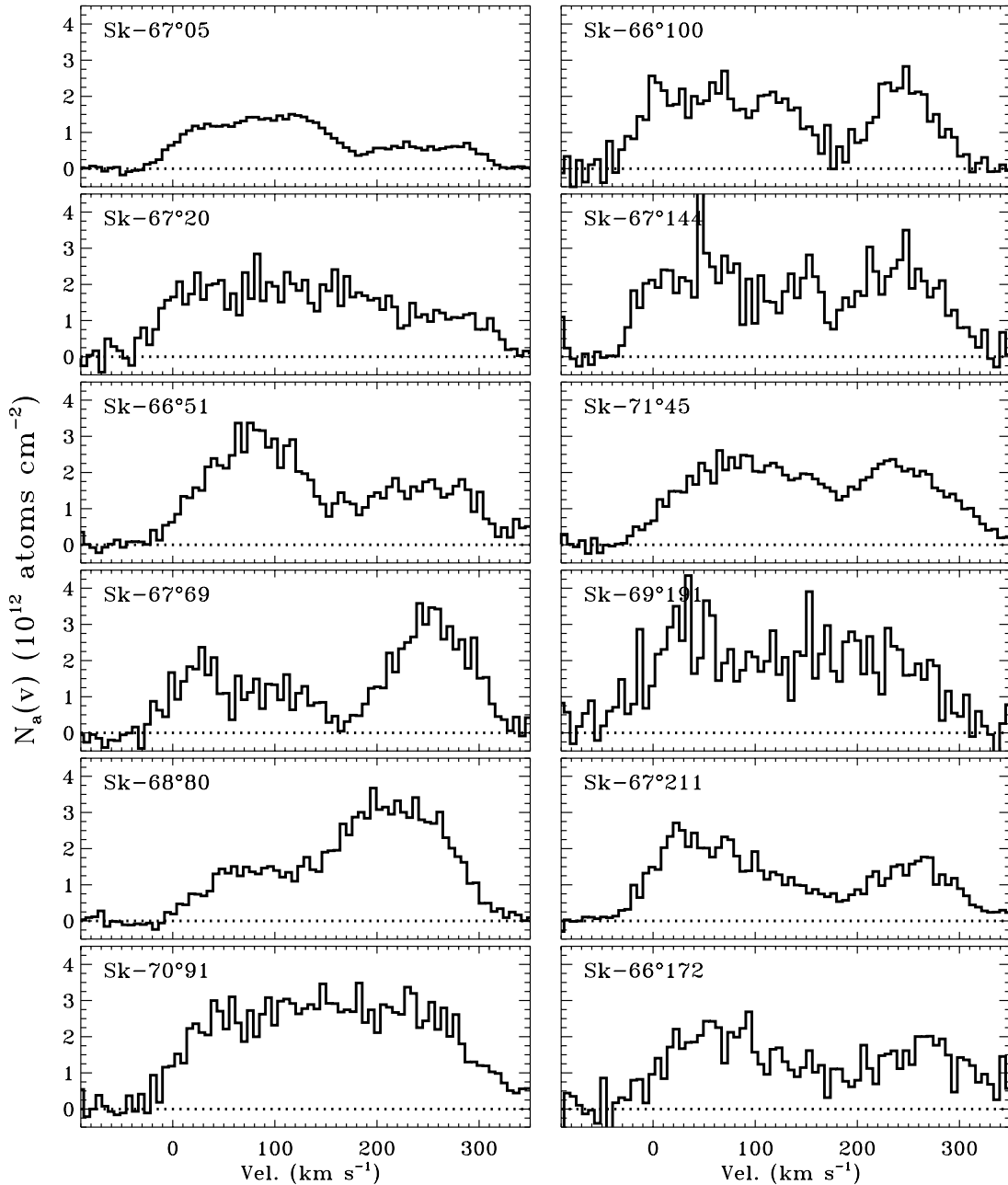


FIG. 1.—Apparent column density, $N_a(v)$, vs. velocity profiles for the sight lines toward the 12 LMC probes discussed in Paper I. The LMC O VI is at velocities $v \geq 175$ km s $^{-1}$. Material at velocities lower than this is associated with the Milky Way and the intermediate- and high-velocity clouds at $v \sim +65$ and $+130$ km s $^{-1}$, respectively.

3. TOTAL O VI COLUMN DENSITIES AND DEGREE-SCALE VARIATIONS

The column densities quoted in Tables 1 and 2 can be seen to vary significantly from sight line to sight line. Toward the LMC the full range of O VI columns spans a factor of ~ 2.8 range when integrated over the full Milky Way velocity limits indicated in the table, or a factor of ~ 4.2 over $|v| \leq 50$ km s $^{-1}$. The SMC sight lines show a factor of ~ 4.2 full range as well.

Figure 3 shows the absolute value of the logarithmic differences in column densities for each pairing of sight lines in our sample, i.e., $|\Delta \log N_{jk}(\text{O VI})| = |\log N_j(\text{O VI}) - \log N_k(\text{O VI})|$ for each pair of LMC sight lines j and k ,

versus the angular separation of the pair, $\Delta\theta_{jk}$. The top panel of this figure shows the difference in O VI column density integrated over the full Milky Way velocity range for each pairing of sight lines, while the bottom panel shows the column density differences when integrating the apparent column density profiles over $|v| \leq 50$ km s $^{-1}$. Figure 4 shows a similar plot for the SMC sight lines.

Figures 3 and 4 demonstrate that there are significant column density variations on all of the angular scales probed by our observations. The smallest separations of LMC sight lines are of order $\Delta\theta_{jk} \sim 0.5^\circ$, while the smallest angular scales probed by the SMC sight lines are $\Delta\theta_{jk} \sim 0.05^\circ$.

Table 3 summarizes the statistics of the O VI column density measurements toward the LMC and SMC. For the

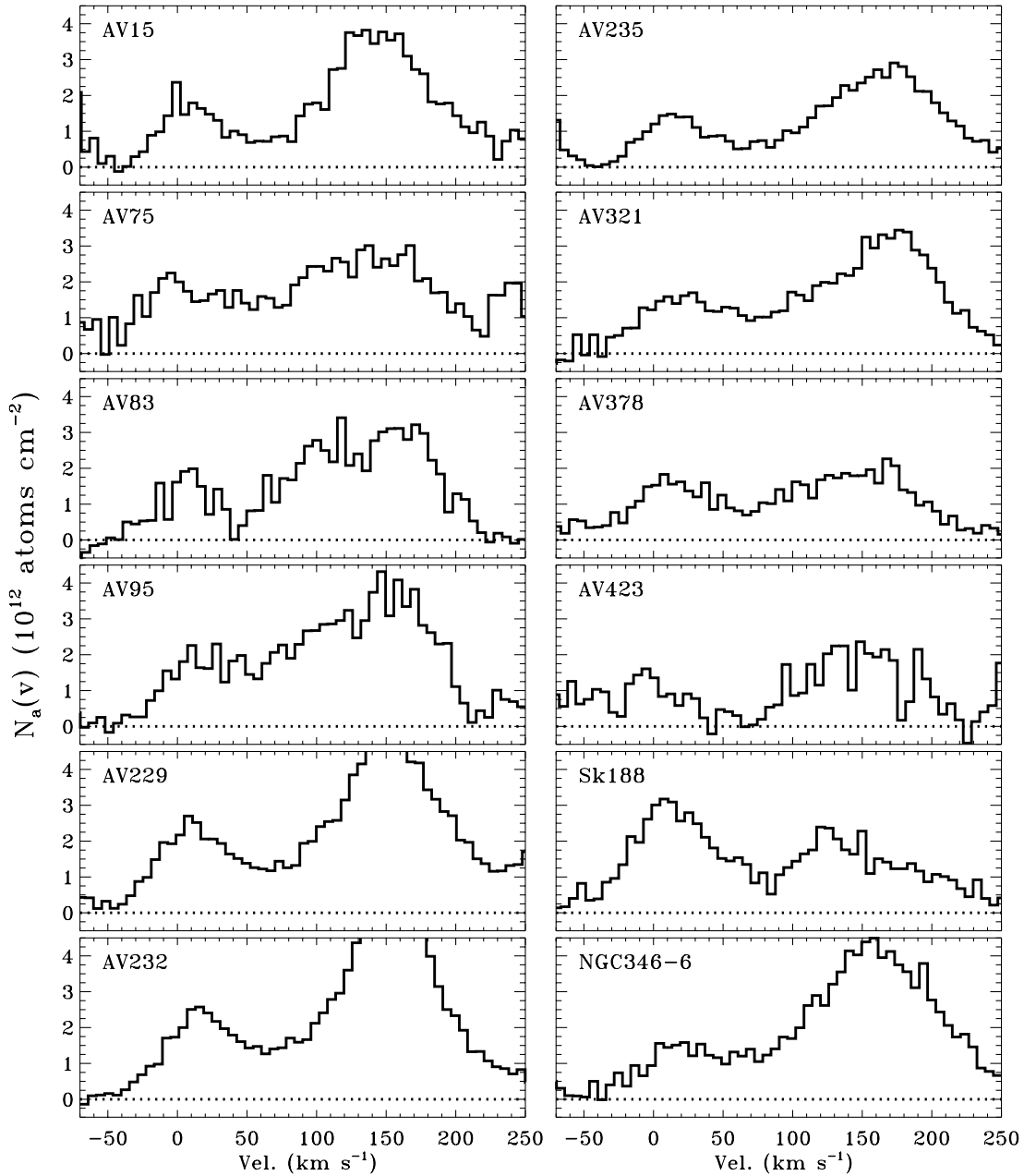


FIG. 2.—Apparent column density, $N_a(v)$, vs. velocity profiles for the sight lines toward 12 of the SMC probes discussed in Paper II. The O VI associated with the SMC is at velocities $v \gtrsim +60 \text{ km s}^{-1}$. Material at velocities lower than this is associated with the Milky Way. The observations of NGC 346-6 include several other early-type stars in the *FUSE* LWRS aperture. The resulting profile has an instrumental line spread function significantly broader than usual for *FUSE* data, and the column density derived for this observation is an average of the individual sight lines contained within the aperture (with the absorption profile weighted by the flux distribution of the targets). We do not make use of the Milky Way column densities derived for the NGC 346 sight lines presented in Paper II in this work.

LMC direction, the results are shown for integrations over the full Milky Way velocity range and over $|v| \leq 50 \text{ km s}^{-1}$, corresponding to the analogous entries in Table 1. Because of the presence of IVCs and HVCs along the LMC sight lines (§ 2.1), the column density differences in the top panel of Figure 3 trace variations in both the low-velocity Milky Way O VI and in the O VI associated with these anomalous-velocity clouds. The IVC and HVC absorption along the LMC sight lines is to a large extent excluded in the integration over the velocity range $|v| \leq 50 \text{ km s}^{-1}$. The variations over this low-velocity material are on average larger than those integrated over the full velocity range (see Table 3).

Indeed, it is interesting to note that the statistics of the LMC and SMC directions are almost indistinguishable if only the low-velocity gas toward the LMC is included.

The standard deviations of the individual O VI column density measurements are a significant fraction of the mean for the LMC and SMC sight lines. Table 3 shows that the standard deviation of each sample is 27%–38% of the mean. For comparison, the standard deviation of the $N(\text{O VI})$ determinations toward 11 bright active galactic nuclei (AGNs) in the study of Savage et al. (2000) is 41% of the mean (with $\log\langle N(\text{O VI}) \rangle = 14.50$). Thus, the LMC/SMC measurements that each sample sight lines within a few

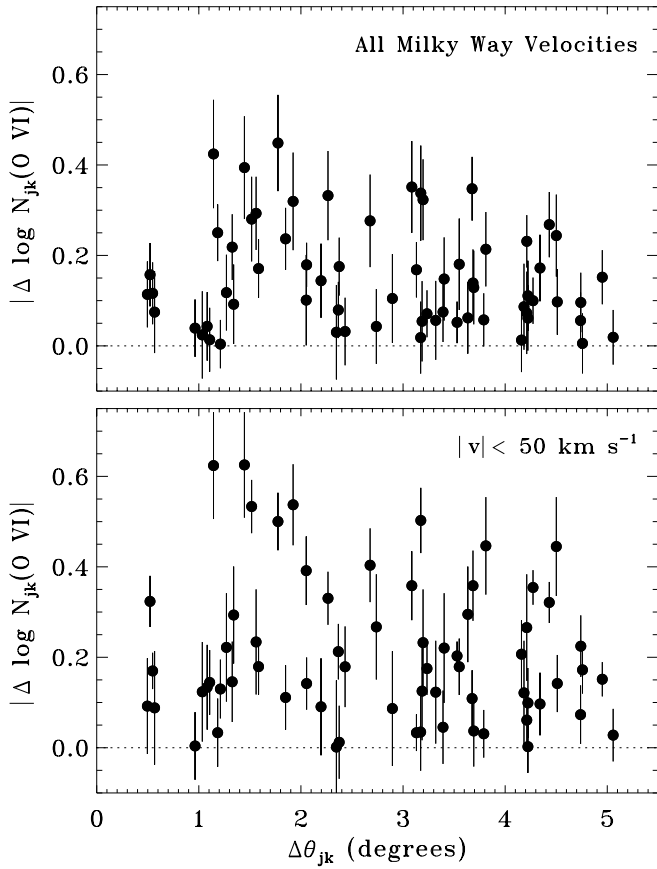


FIG. 3.—Absolute logarithmic difference in O VI column densities for each pair of sight lines in Table 1. The top panel shows the difference in O VI column density integrated over the full velocity ranges quoted in Table 1 for each pair of sight lines. The bottom panel shows the column density differences when integrating the apparent column density profiles over the range $-50 \text{ km s}^{-1} \leq v \leq +50 \text{ km s}^{-1}$, which excludes much of the expected intermediate- and all of the expected high-velocity cloud absorption.

degrees of one another show an amount of (fractional) variation that is similar to that seen along sight lines distributed across the entire celestial sphere. Indeed, compared with the uncertainties in the individual measurements, the variation

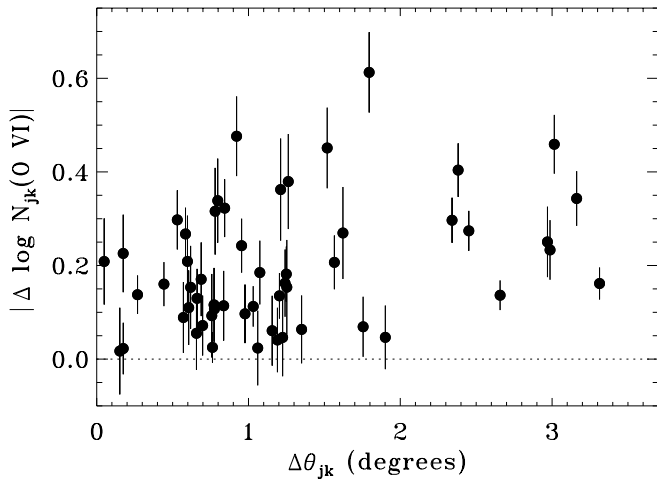


FIG. 4.—Absolute logarithmic difference in O VI column densities for each pair of SMC sight lines in Table 2.

TABLE 3
STATISTICAL PROPERTIES OF GALACTIC HALO O VI TOWARD THE LMC AND SMC

PROPERTY	LMC		SMC (v_-, v_+)
	($-50, +50$) ^a	(v_-, v_+) ^b	
$\log \langle N(\text{O VI}) \rangle$	14.06	14.52	14.13
$\log \langle N(\text{O VI}) \sin b \rangle$	13.80	14.26	13.97
$\sigma_{N(\text{O VI})} / \langle N(\text{O VI}) \rangle$ (%) ^c	36	27	38
$\langle \Delta \log N(\text{O VI}) \rangle$ ^d	0.21	0.15	0.20
Max $ \Delta \log N(\text{O VI}) $	0.62	0.45	0.62

^a This column describes the statistics of the Galactic halo O VI column densities in the direction of the LMC when integrated over velocities $|v| \leq 50 \text{ km s}^{-1}$.

^b This column describes the statistics of the Galactic halo O VI column densities in the direction of the LMC when integrated over the full range v_-, v_+ given in Table 1.

^c The standard deviation of the measurements compared with the mean (given in percent).

^d The average value of $|\Delta \log N(\text{O VI})_{jk}| \equiv |\log N_j(\text{O VI}) - \log N_k(\text{O VI})|$ for all pairs of sight lines j and k .

between the LMC and SMC sight lines is more significant than that in the Savage et al. (2000) data set (as judged by the values of χ^2 derived by comparing the data with the mean within each sample).

Figures 3 and 4 show that significant variations in the O VI column densities of the Galactic halo ($|\Delta \log N_{jk}(\text{O VI})| > 0$ at greater than 2σ significance) can be found for sight lines over the entire range of angular scales probed by our observations. This includes pairs of sight lines separated by $\lesssim 1^\circ$, many of which show greater than 0.1 dex ($\sim 25\%$) variations.

To demonstrate the degree of variation of and any systematics in the distribution of column densities, Figures 5

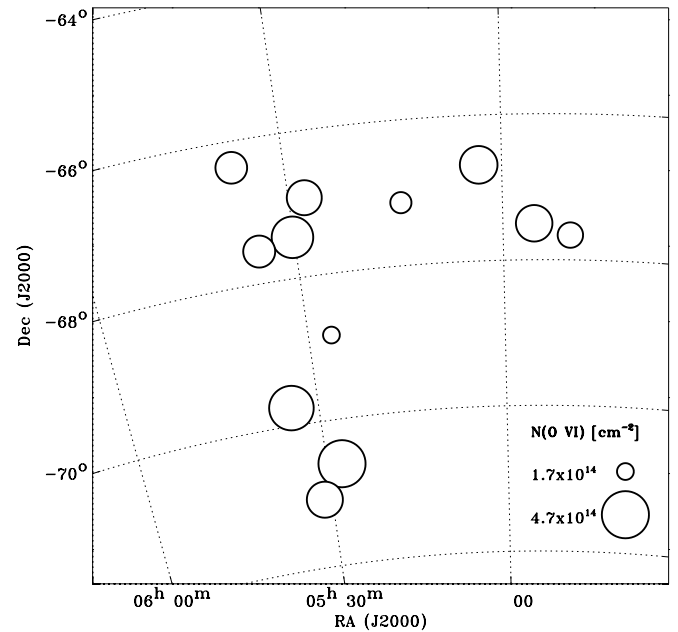


FIG. 5.—“Map” of the integrated Galactic O VI column densities observed toward 12 LMC probes. Each circle is centered on the background star and has a radius linearly proportional to the integrated Milky Way O VI column. For scale, circles denoting the minimum and maximum O VI columns are shown in the bottom right.

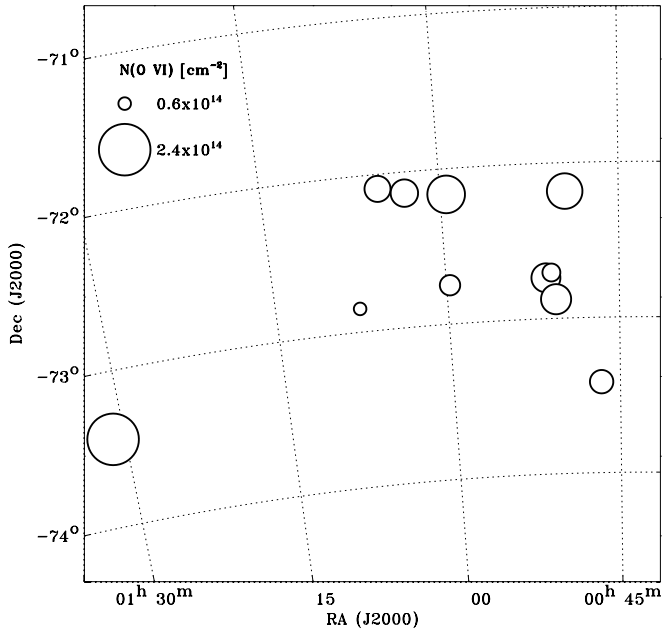


FIG. 6.—As Fig. 5, but for the 11 SMC sight lines, with the scale shown at the upper left.

and 6 show “maps” of the derived Galactic O VI column densities toward the LMC and SMC, respectively. The positions of the probe stars are marked with circles whose radii are linearly proportional to the column densities summarized in Tables 1 and 2. Scales showing the minimum and maximum columns are given. With only 12 and 11 sight lines, the maps are too sparsely populated to say whether or not coherent structures are visible in our data.

Figure 7 shows the angular autocorrelation function (ACF), $w(\theta)$, for the O VI column densities toward the LMC and SMC. The ACF was calculated in a manner analogous to the studies of the X-ray sky by Chen et al. (1994) and Kuntz et al. (2001). We define the ACF as

$$w(\theta) \equiv \frac{\sum_i \sum_{j \neq i} (N_i - \langle N \rangle)(N_j - \langle N \rangle)(\sigma_i \sigma_j)^{1/2}}{\langle N \rangle^2 \sum_i \sum_{j \neq i} (\sigma_i \sigma_j)^{1/2}}. \quad (1)$$

The summation is calculated for each pair of sight lines i and j separated by an angle θ on the sky. In this expression N_i and N_j are the O VI column densities and σ_i and σ_j are the column density uncertainties for the sight lines, while $\langle N \rangle$ is the average column density for the entire sample of 12 or 11 stars. The $w(\theta)$ data displayed in Figure 7 have been summed over 0.6° bins for the LMC data set; the summation for the SMC data set is over 0.3° bins for separations smaller than 2° and 0.6° bins for larger angular separations. The uncertainties in $w(\theta)$ represent 95% confidence limits. These were determined through 1000 simulations wherein the column densities were randomly shuffled among the observed directions and $w(\theta)$ rederived, similar to the method described by Carrera et al. (1991). The confidence limits shown in Figure 7 include 95% of the simulated $w(\theta)$ values. This approach to estimating uncertainties has the advantage that the simulated data are drawn from the same population as the real data, and hence no intrinsic column density distribution function need be assumed. To remove any systematic effects from the ACF, we have subtracted the mean

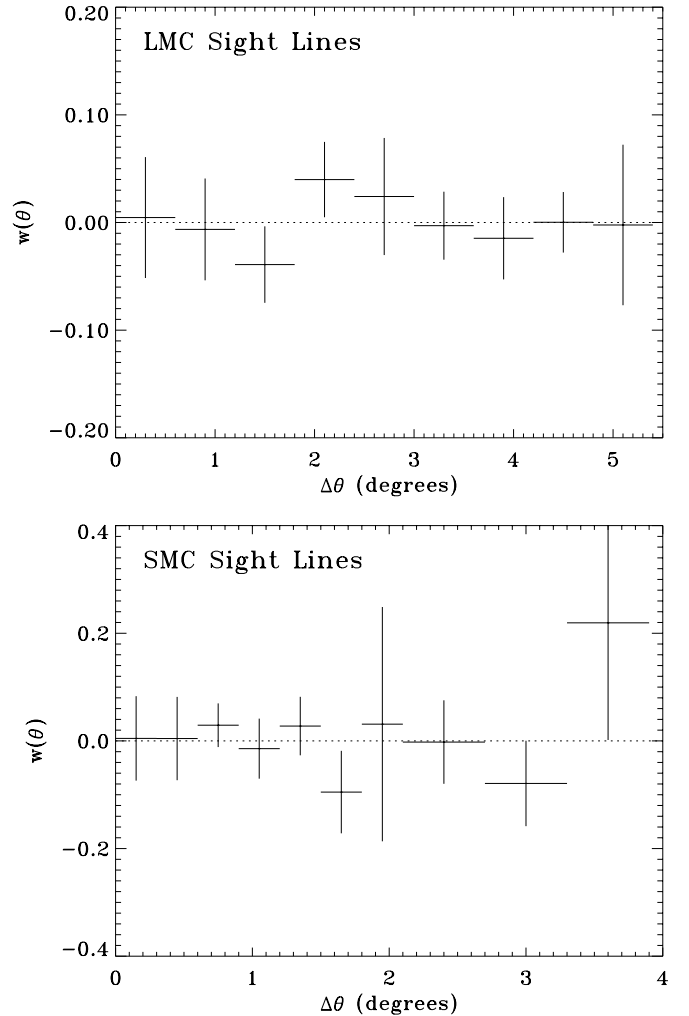


FIG. 7.—Autocorrelation function, $w(\theta)$, for the O VI column densities toward the LMC (*top*) and SMC (*bottom*) derived as described in the text. The bin spacing for the LMC points is 0.6° . The bin spacing for the SMC points is 0.3° and 0.6° for angular separations less than and greater than 2° , respectively. The uncertainties are calculated using simulations (see text) and represent 95% confidence intervals.

simulated $w(\theta)$ from the real values, although the mean simulated values were always very small compared with the uncertainties.

Figure 7 shows that there is little evidence for significant power at any scale in the ACF for the O VI column densities toward the LMC and SMC. Indeed, those points that seem to be different from $w(\theta) = 0$ are not robust to changes in the bin spacing. When binned over the same angular scale, the LMC and SMC $w(\theta)$ values are completely consistent over all scales probed.

There is no evidence for significantly greater power in the ACFs on small angular scales compared with large scales along these two sight lines. We caution that the small number of sight lines makes the uncertainties large over all scales. Furthermore, the ACFs are insensitive to structure on scales smaller than the adopted bin size for each sight line. Thus, both larger numbers of sight lines and finer sampling would be needed to probe the smallest structures. However, our data could be used with further measurements of O VI toward AGNs to constrain the largest scale O VI structures in the sky.

4. KINEMATICS OF GAS IN THE GALACTIC HALO

The kinematic profiles of the O VI absorption lines toward the LMC and SMC could, in principle, yield information on the distribution of gas in the Galactic halo assuming it corotates with the underlying thin disk and adopting an appropriate rotation curve (see, e.g., Savage & de Boer 1981; Savage, Sembach, & Lu 1997). Examining the distribution of apparent column density versus velocity for LMC and SMC sight lines in this manner can yield estimates of the turbulent velocity, midplane density, and scale height of the absorbing layer.

There are several caveats to this approach for the particular sight lines studied here, however. Figure 8 shows a comparison of the apparent column density, $N_a(v)$, profiles of O VI and Fe II (derived from the 1125.448 Å transition) for

the sight lines toward Sk $-67^\circ 211$ and Sk $-68^\circ 80$ in the LMC. The Fe II absorption mostly traces gas associated with the neutral ISM (i.e., H I-bearing gas). Also shown is the Clemens (1985) rotation curve for the direction of the LMC.⁵ These plots demonstrate the difficulty in analyzing the O VI kinematics in this direction. Although the sharp Fe II absorption in the main Milky Way component suggests the Fe II-bearing material is confined to relatively small distances from the midplane (consistent with the results of Edgar & Savage 1989), determining the extent of the Milky

⁵ The reader should be aware that the velocities presented in the O VI and Fe II profiles are expected to be accurate to $\pm 10\text{--}15$ km s $^{-1}$ when comparing the observed profiles with the displayed rotation curve.

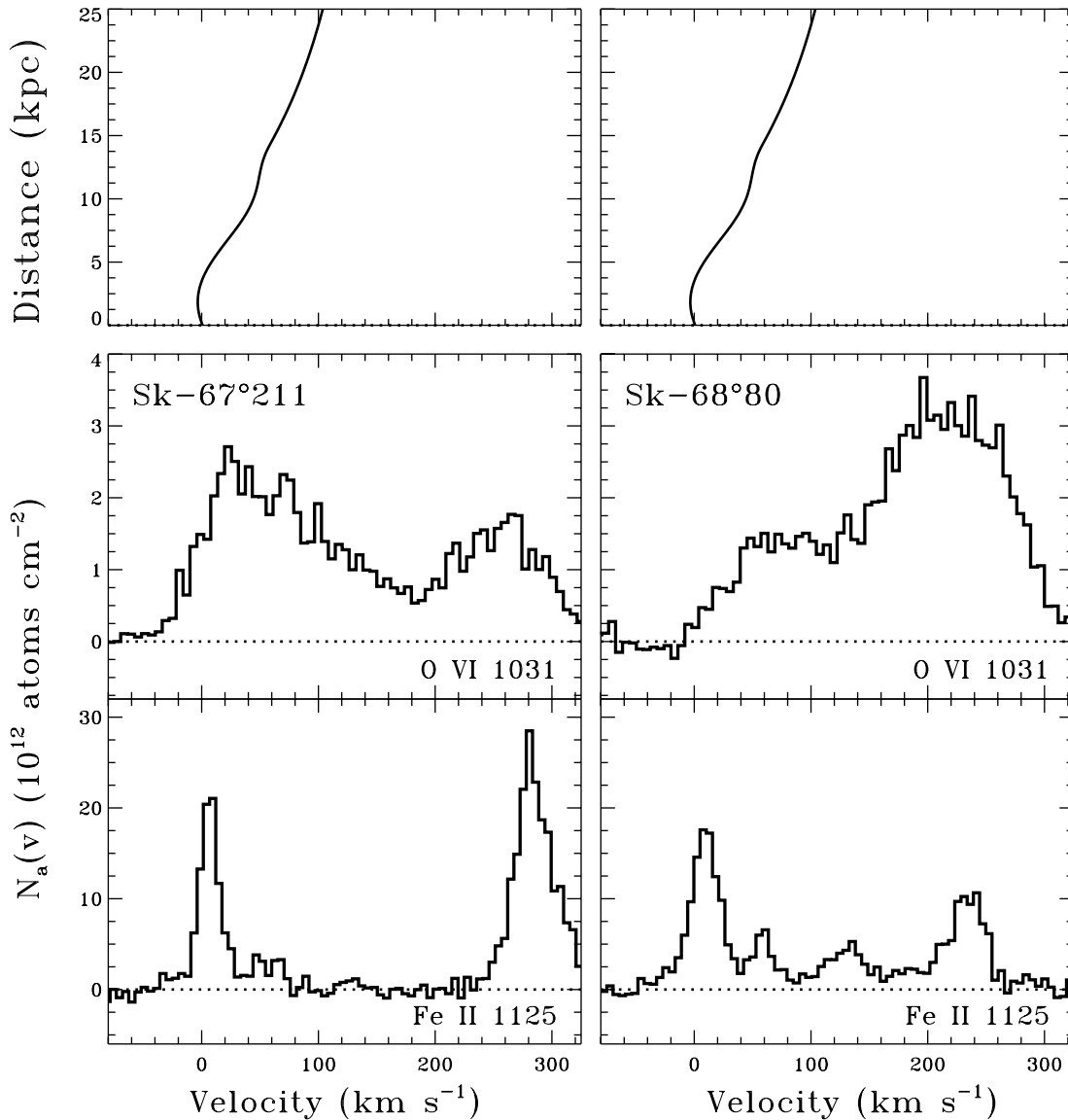


FIG. 8.—Apparent column density profiles for interstellar O VI and Fe II toward the stars Sk $-67^\circ 211$ and Sk $-68^\circ 80$ in the LMC (separated by $1^\circ 5$ on the sky). Also shown in the top panel is the Galactic rotation curve as a function of distance from the Sun in the direction of the LMC from (Clemens 1985). Absorption from intermediate- and high-velocity clouds can be seen in the Fe II profiles toward both stars (the weak high-velocity absorption toward Sk $-67^\circ 211$ is confirmed in stronger Fe II transitions). The apparent column density profiles are likely lower limits in the cores of the Fe II lines due to the presence of unresolved saturated structure.

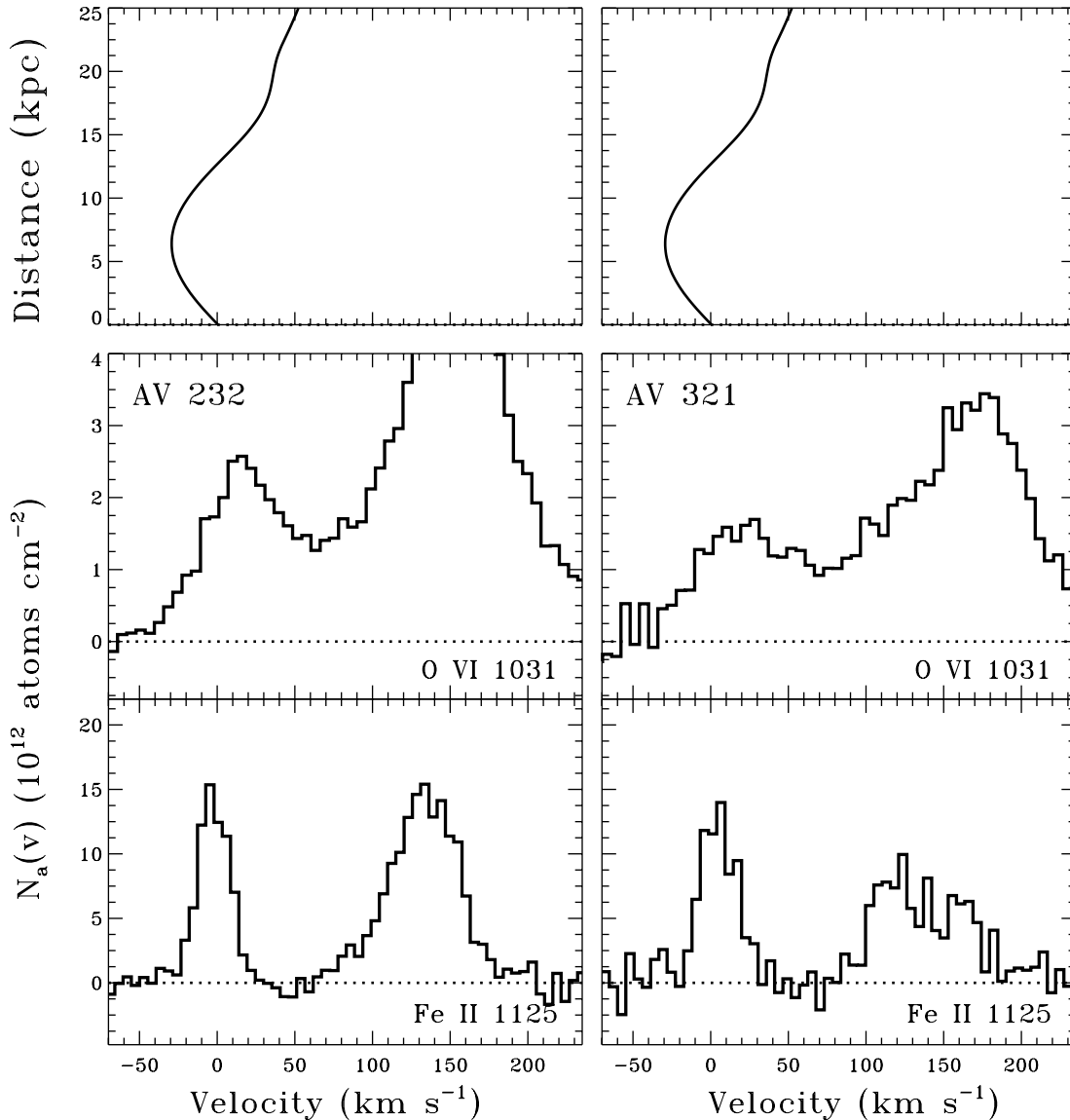


FIG. 9.—Apparent column density profiles for interstellar O VI and Fe II toward the stars AV 232 and AV 321 in the SMC (separated by $0^{\circ}3$ on the sky). Also shown in the top panel is the Galactic rotation curve as a function of distance from the Sun in the direction of the SMC from (Clemens 1985). The apparent column density profiles are likely lower limits in the cores of the Fe II lines due to the presence of unresolved saturated structure.

Way halo O VI absorption is difficult given the overlap with IVC, HVC, and LMC material.

Furthermore, examining Figure 8 shows that the O VI $N_a(v)$ profiles for these two sight lines are significantly different at even low velocities, i.e., velocities that should be free from contamination by IVC and HVC contamination. The Sk $-67^{\circ}211$ sight line shows much larger apparent column densities over all velocities $v \leq +50$ km s^{-1} than the sight line toward Sk $-68^{\circ}80$. Furthermore, the shape of the profiles is quite different over the lowest velocities, with the Sk $-67^{\circ}211$ profile exhibiting a sharp peak at low positive velocities and significant absorption at negative velocities (neither of which are easily identified along the Sk $-68^{\circ}80$ sight line). Given the differences seen between the two LMC sight lines examined above, which are separated by $1^{\circ}5$ on the sky, models of smooth, plane-parallel halo material corotating with the underlying Galactic disk do not appropri-

ately describe the complicated nature of the observed O VI profiles.

Figure 9 shows the O VI and Fe II profiles for the stars AV 232 and AV 321 in the SMC. These stars are separated by only $0^{\circ}3$ on the sky, and again significant variations between the sight lines are seen at low velocity in the O VI $N_a(v)$ profiles. The two $N_a(v)$ profiles exhibit differences not only in the peak and total O VI column densities, but also in the velocity distribution of the gas. While there is no clear evidence for IVC absorption in these directions (although Welty et al. 1997 have found weak IVC absorption in the direction of the SMC star Sk 108), absorption associated with the SMC begins to overlap the Milky Way absorption at velocities nearing $+100$ km s^{-1} . The low-velocity tail of the broad O VI distribution in the SMC likely overlaps the Galactic O VI at velocities below this.

While the derivation of reliable estimates of scale height, midplane densities, and turbulent velocities using the O VI

absorption in these directions may give ambiguous results, examination of the kinematic profiles of Milky Way O VI seen toward the Magellanic Clouds does lead to several important conclusions regarding the nature of highly ionized Galactic halo gas. That the individual absorbing components are seen more distinctly in the Fe II profiles (Fig. 8) implies that the O VI absorption contains more and/or broader component complexes than the Fe II. This is consistent with our expectations given the temperature of the gas the two species are thought to trace.

In the direction of the SMC, the Milky Way O VI absorption is clearly broader than the Fe II absorption. This suggests that the O VI arises in a layer much more extended than that traced by Fe II, which has a vertical extension similar to that of H I (Edgar & Savage 1989). Toward the LMC, the fraction of the gas arising at velocities associated with IVC and HVC absorption is quite different for the O VI and Fe II profiles. A larger fraction of the O VI absorption is found at high velocities. Given that the IVC and HVC material toward the LMC likely resides far from the Galactic plane, this implies that a greater fraction of the O VI is found in the Galactic halo than Fe II.

This all suggests that while the O VI-bearing medium is quite inhomogeneous, the current observations certainly suggest the O VI layer of the Galaxy is significantly different than the Fe II-bearing layer. O VI is found at preferentially larger distances from the Galactic plane than is the Fe II. Stated another way, the effective scale height of the O VI-bearing gas is larger than that of the Fe II-bearing material.

5. DISCUSSION

We have presented measurements of O VI in the Galactic halo observed toward early-type stars in the LMC and the SMC. These show significant O VI column density variations on degree scales (and smaller) over velocity ranges corresponding to gas in the Galactic disk and halo. The dispersion of halo O VI measurements is $\sim 27\%$ to $\sim 38\%$ of the averages in these directions. The ratio of the highest to lowest O VI column densities ranges from 2.8 to 4.2, with the latter applying to the low-velocity gas toward the LMC and the entire Milky Way range toward the SMC.

Several properties of O VI in the Galactic halo can be inferred from the properties of these sight lines toward the Magellanic Clouds. The most fundamental inference to be drawn from our observations is that the O VI-bearing medium of the Galactic halo is better described by spatially patchy distribution than by a smooth layer (e.g., like that discussed by Spitzer 1956). That the medium is patchy favors models in which the O VI resides in clouds of 3×10^5 K material or in the interfaces between cooler ($< 10^5$ K) clouds and a hotter ($\gtrsim 10^6$ K) medium. The evidence for this conclusion comes both from the observed column density variations and the kinematic differences between sight lines (see Figs. 1 and 2).

The greater velocity breadth of O VI than Fe II in the direction of the SMC and the much larger contribution of intermediate- and high-velocity halo clouds to the O VI profiles than to the Fe II profiles toward the LMC imply that the Galactic O VI in these directions is extended further from the plane than the Fe II. Effectively, these inferences imply the scale height of Galactic O VI is larger than that of Fe II. Although the models of smoothly distributed, exponentially stratified gas layers assumed for determining the properties

of the O VI layer seem inappropriate (§ 4), our data do require that the Galactic O VI and Fe II be distributed in very different ways.

That the Galactic halo O VI-bearing medium is poorly described by a smoothly distributed layer of gas is a conclusion one must also draw from the Savage et al. (2000) observations of O VI absorption toward extragalactic FUV sources. However, the current observations show that the distribution of O VI within the halo must have significant variations over much smaller angular, and hence physical, scales. To what physical scales might the observed variations correspond? The distribution of O VI absorption seems to be more tightly concentrated toward the Galactic mid-plane than that of C IV and Si IV (Savage et al. 2000). The latter ions have distributions with best-fit scale heights of ~ 4.4 and 5.1 kpc (Savage et al. 1997)—under the assumption that an exponentially stratified layer with some degree of irregularities (patchiness) is a good description of the intrinsic distribution. If we assume that the observed O VI absorption in the Galactic halo toward the Magellanic Clouds resides at heights lower than $z \sim 5$ kpc (i.e., within one Si IV scale height), then the $0^\circ 5' - 5^\circ 0'$ scales probed by our LMC observations correspond to linear distances of $\ll 80 - 800$ pc while the $0^\circ 05' - 3^\circ 3'$ scales probed by the SMC measurements correspond to distances of $\ll 6 - 400$ pc. Much of the gas is likely to be significantly closer to the Sun than this limit, making these estimated size scales upper limits. In particular, if the effective scale height of the O VI distribution is $h_z \sim 2.7$ kpc (as derived by Savage et al. 2000), then $\sim 85\%$ of the Galactic O VI is expected to be at heights smaller than the adopted 5 kpc.

If we assume that the O VI variations are due to clouds at this ~ 5 kpc distance from the plane with angular sizes approximately equal to the transverse separation of the pairing of stars observed (giving physical sizes of $80 - 800$ pc toward the LMC and $5 - 400$ pc toward the SMC), we can estimate the required densities of O VI for the observed column density differences between the sight lines. The mean density derived under these assumptions is $\langle n_{\text{O VI}} \rangle \sim 1.5 \times 10^{-7} \text{ cm}^{-3}$ for the LMC sight lines with significant ($\geq 2\sigma$) column density differences; the full range of densities is $\sim (0.4 - 4.4) \times 10^{-7} \text{ cm}^{-3}$. Toward the SMC the mean density derived in this manner is $\langle n_{\text{O VI}} \rangle \sim 2.7 \times 10^{-7} \text{ cm}^{-3}$ with a full range of $\sim (0.6 - 27) \times 10^{-7} \text{ cm}^{-3}$. These values give estimated particle densities of $\langle n_{\text{H}} \rangle \sim 1.4 \times 10^{-3}$ and $\sim 2.5 \times 10^{-3} \text{ cm}^{-3}$ for the LMC and SMC directions, respectively, assuming the abundance of oxygen relative to hydrogen is 5.5×10^{-4} (Holweger 2001) and the fraction of oxygen in the form of O^{+5} is $\lesssim 0.2$ (Sutherland & Dopita 1993).

The average density estimates can be used to estimate the pressure of the O VI-bearing gas. For $P/k = nT = 2.3n_{\text{H}}T$, where the factor of 2.3 allows for the total number of particles in a fully ionized gas containing 10% helium, we obtain $\langle P/k \rangle \sim 10^3$ to $1.7 \times 10^3 \text{ K cm}^{-3}$ for the directions to the LMC and SMC, respectively. These estimates adopt the average densities derived in the previous paragraph, and we have assumed $T = 3 \times 10^5 \text{ K}$, the temperature where O VI peaks in abundance in collisional ionization equilibrium. The densities and pressures derived in this way will be higher for clouds closer than the assumed 5 kpc height from the plane of the Galaxy.

This approach to estimating densities and pressures is overly simplistic, and we caution the reader not to put too

much emphasis on these idealized calculations—neither the true distances to nor the morphology of the absorbing material is known. If the morphology of the O VI-bearing ISM is more sheetlike or filament-like, then much of the variation in column density will be the result of the projection of the individual absorbing components along the line of sight (see, e.g., Heiles 1997). Indeed, the interpretation of the absorption arising in individual clouds at a common distance is highly unsatisfactory given the apparent lack of any preferred scales for the observed variability.

We suggest that the observations presented in this work, which show degree-scale column density and kinematic variations in the O VI-bearing medium of the Galactic halo, fit readily into pictures of the Galactic halo wherein the O VI is contained in complicated cloudlike or sheetlike distributions of material. In particular, models that place the O VI gas in interfaces between more neutral clouds or sheets and a more pervasive very hot ($\geq 10^6$ K) ISM would seem to allow for the observed variations so long as there are not so many such interfaces along typical paths through the halo that the expected variations along random adjacent sight lines is expected to be small.

The morphological information contained in the absorption-line data sets presented here is incomplete, probing only random pencil beams through the highly ionized halo. With our sparsely populated “maps” it is difficult to discern the structure of the halo O VI. Our observations do give the first hint of the complexity of the small-scale distribution of hot, highly ionized material within the halo. The structures giving rise to the O VI column density variations demonstrated in this work will be accessible to future O VI emission-line imaging programs. Indeed, that we find significant variations on the smallest angular scales probed suggests there is a wealth of structure present in the highly ionized sky; imaging data may reveal how this highly ionized material is related to other phases of the ISM.

We also note that the degree of structure demonstrated by our O VI absorption measurements has important implications for understanding current observations of diffuse O VI emission. The comparison of O VI emission-line intensities with the O VI column density along the same line of sight can yield estimates of the physical properties of the O VI-bearing gas, e.g., the density and pressure (Shelton et al. 2001; Dixon et al. 2001). However, the determination of the appropriate column density for comparison with an emission-line measurement is difficult. Our observations (e.g., Figs. 3 and 4) suggest that O VI absorption-line measurements along sight lines even a few arcminutes from the direction of an emission-line measurement can only be assumed to yield column densities within a factor of approximately 2 of the value appropriate for the emitting region. The large degree of variation in the absorption-line column densities along closely spaced sight lines through the Galactic halo must be considered when assessing the systematic uncertainties in comparing emission and absorption-line measurements of O VI. However, one may look at this in another way: our analysis suggests that sight lines several

degrees apart give column densities that are expected, on average, to give results that are no less consistent than sight lines separated by less than a degree. That is, unless the opportunity exists to observe O VI emission and absorption along essentially the same sight line, the determination of an O VI column density several degrees away from an emission-line measurement will provide no worse an indicator than an O VI column density determined for a sight line tens of arcminutes away.

6. SUMMARY

We have presented observations of Galactic halo O VI absorption toward 12 and 11 early type stars in the Large and Small Magellanic Clouds, respectively. These observations reveal strong column density variations on degree scales. The principle results of this study are as follows.

1. The Galactic halo O VI probed by our observations shows significant structure on all of the scales probed by our observations (0.05° – 5°). There seems to be no preferred angular scale for O VI variations over this range. The transverse size scales probed by our observations are likely ≤ 6 – 800 pc.

2. The Galactic O VI in the directions of the Magellanic Clouds is very patchy, with the standard deviations of the measurements being equivalent to $\sim 26\%$ – 38% of the average values in these directions. The maximum variations correspond to factors of ~ 2.9 – 4.2 .

3. Galactic O VI is distributed in a very different manner than Fe II. The O VI-bearing layer of the Galaxy is significantly more extended than the Fe II-bearing layer, which has a vertical extent similar to that of H I. However, the existence of large variations in the O VI column densities over very small angular scales implies that models of a smoothly varying, exponentially stratified halo are poor descriptions of the true distribution of highly ionized gas. The meaning of detailed quantities derived by comparing such models with the observed O VI kinematics along a given sight line (or sight lines) is ambiguous at best.

4. The existence of large column density variations over small angular scales can be used to constrain the origin of Galactic halo O VI ions. Models in which the O VI-bearing medium is composed of complicated cloud- or sheetlike distributions of material (particularly narrow interfaces) should be considered more likely than smoothly distributed layers of highly ionized material in light of our observations.

This work is based on data obtained for the Guaranteed Time Team by the NASA-CNES-CSA *FUSE* mission, operated by the Johns Hopkins University. Financial support to US participants has been provided by NASA contract NAS 5-32985. J. C. H. and K. R. S. recognize support from NASA Long-Term Space Astrophysics grant NAG 5-3485 through the Johns Hopkins University.

REFERENCES

- Bomans, D. J., de Boer, K. S., Koornneef, J., & Grebel, E. K. 1996, *A&A*, 313, 101
- Carrera, F. J., Barcons, X., Butcher, J. A., Fabian, A. C., Stewart, G. C., Warwick, R. S., Hayashida, K., & Kii, T. 1991, *MNRAS*, 249, 698
- Chen, L.-W., Fabian, A. C., Warwick, R. S., Branduardi-Raymont, G., & Barber, C. R. 1994, *MNRAS*, 266, 846
- Clemens, D. P. 1985, *ApJ*, 295, 422
- Danforth, C. W., Howk, J. C., Fullerton, A. W., Blair, W. P., & Sembach, K. R. 2002, *ApJS*, 139, 230
- Dixon, W. V., Sallmen, S., Hurwitz, M., & Lieu, R. 2001, *ApJ*, 552, L69
- Edgar, R. J., & Savage, B. D. 1989, *ApJ*, 340, 762
- Ferlet, R., Dennefeld, M., & Maurice, E. 1985, *A&A*, 152, 151

- Fitzpatrick, E. L. 1984, *ApJ*, 282, 436
Fitzpatrick, E. L., & Savage, B. D. 1983, *ApJ*, 267, 93
Friedman, S. D., et al. 2000, *ApJ*, 538, L39
Heiles, C. 1997, *ApJ*, 481, 193
Holweger, H. 2001, in *AIP Conf. Proc. 598, Solar and Galactic Composition*, ed. R. F. Wimmer-Schweingruber (Melville: AIP), 23
Hoopes, C. G., Sembach, K. R., Howk, J. C., & Blair, W. P. 2001, *ApJ*, 558, L35
Hoopes, C. G., Sembach, K. R., Howk, J. C., & Savage, B. D. 2002, *ApJ*, submitted
Howk, J. C., Sembach, K. R., Savage, B. D., Massa, D., Friedman, S. D., & Fullerton, A. W. 2002, *ApJ*, 569, 214
Koenigsberger, G., et al. 2001, *AJ*, 121, 267
Kuntz, K. D., Snowden, S. L., & Mushotzky, R. F. 2001, *ApJ*, 548, L119
Mallouris, C., et al. 2001, *ApJ*, 558, 133
McGee, R. X., Newton, L. M., & Morton, D. C. 1983, *MNRAS*, 205, 1191
Murphy, E. M., et al. 2000, *ApJ*, 538, L35
Oegerle, W. R., et al. 2000, *ApJ*, 538, L23
Savage, B. D., & de Boer, K. S. 1979, *ApJ*, 230, L77
———. 1981, *ApJ*, 243, 460
Savage, B. D., Jenkins, E. B., Joseph, C. L., & de Boer, K. S. 1989, *ApJ*, 345, 393
Savage, B. D., & Sembach, K. R. 1991, *ApJ*, 379, 245
Savage, B. D., Sembach, K. R., & Lu, L. 1997, *AJ*, 113, 2158
Savage, B. D., et al. 2000, *ApJ*, 538, L27
Sembach, K. R., & Savage, B. D. 1992, *ApJS*, 83, 147
Sembach, K. R., et al. 2000, *ApJ*, 538, L31
Sfeir, D. M., Lallement, R., Crifo, F., & Welsh, B. Y. 1999, *A&A*, 346, 785
Shelton, R. L., et al. 2001, *ApJ*, 560, 730
Spitzer, L. 1956, *ApJ*, 124, 20
Sutherland, R. S., & Dopita, M. A. 1993, *ApJS*, 88, 253
Wakker, B. P., Howk, J. C., Chu, Y.-H., Bomans, D., & Points, S. D. 1998, *ApJ*, 499, L87
Welty, D. E., Frisch, P. C., Sonneborn, G., & York, D. G. 1999, *ApJ*, 512, 636
Welty, D. E., Lauroesch, J. T., Blades, J. C., Hobbs, L. M., & York, D. G. 1997, *ApJ*, 489, 672
Widmann, H., et al. 1998, *A&A*, 338, L1
Yan, Z.-C., Tambasco, M., & Drake, G. W. F. 1998, *Phys. Rev. A*, 57, 1652